Solving Phase-Noise Fokker–Planck Equations Using the Motion-Group Fourier Transform

Yunfeng Wang, *Member, IEEE*, Yu Zhou, *Member, IEEE*, David Keith Maslen, and Gregory S. Chirikjian, *Member, IEEE*

***Abstract*—A quantity of importance in coherent optical communications is the probability density of a filtered signal in the presence of phase noise (PN). The Fokker–Planck (FP) approach has been recognized as a rigorous way to describe these statistical properties. However, computational difficulties in solving these FP equations have prevented their widespread application. In this paper, we present a new and simple computational solution method based on techniques from noncommutative harmonic analysis on motion groups. This proposed method can easily solve all the PN FP equations with any kind of intermediate frequency filter. We also present a new derivation of PN FP equations from the viewpoint of stochastic processes.**

***Index Terms*—Coherent optical communications, Fokker–Planck (FP) equations, motion groups, phase noise (PN), stochastic processes.**

I. Introduction

LASER phase noise (PN) puts strong limitations on the performance of coherent optical communication systems. Evaluating the influence of laser PN is essential in the system design and optimization, and has been studied extensively in the literature. Analytical models that describe the relationship between PN and the filtered signal are found in [1], [6], [7], [10], [13], [18], and [22]. In particular, the Fokker–Planck (FP) approach represents the most rigorous description of PN effects [5], [10], [18], [22]. In this approach, the probability density function (PDF) of the filtered signal can be obtained as the solution of FP equations.

There are two types of PN FP equations. One is a three-state-variable (i.e., 3-D) FP equation which provides complete statistical information on both the filtered signal and PN. According to the literature cited above, it is extremely hard to solve this 3-D FP equation. To circumvent this computational complexity, a two-state-variable (i.e., 2-D) FP equation is derived by suppressing the dimension on PN. By only considering a finite time integrator (integrate-and-dump filter), a number of papers have attempted to solve this 2-D FP equation using a variety of techniques, including series expansions [6], numerical methods based on discretizing the domain [19], approximation methods [18], and analytical methods [22]. All of them are based on classical partial differential-equation solution techniques and have difficulties to solve the FP equations for other types of intermediate frequency (IF) filters. The computational difficulty of this FP approach has prohibited its effective and broad application.

In this paper, we present a new computational method that can easily solve both 2-D and 3-D FP equations with any kind of IF filters. Our method relies on techniques from group theory (and, in particular, noncommutative harmonic analysis on groups, as developed in [3]). Using these techniques, these FP equations are converted into a system of linear ordinary differential equations (ODEs) with constant or time-varying coefficients in a generalized Fourier space. These ODEs can be easily solved by either a matrix exponential (for constant coefficients) or Runge–Kutta integration (for time-varying coefficients). Our method removes the computational difficulty of the FP approach.

We believe that the powerful techniques of noncommutative harmonic analysis are efficient and natural for this problem. We also believe that by introducing the community of researchers working on optical communication systems to techniques of noncommutative harmonic analysis, other computational and analytical problems which currently appear to be intractable may also lend themselves to straightforward solution.

II. Phase Noise Fokker–Planck Equations

The phase of the light emitted from a semiconductor laser exhibits random fluctuations due to spontaneous emissions in the laser cavity. This phenomenon is commonly referred to as PN. Because there are only about 10^4 photons in the active region of a semiconductor laser, the phase of the light is significantly perturbed by just one spontaneous photon. To evaluate the influence of PN on coherent optical communication systems, the main issue is to find the statistical characterization of the output of the IF filter corrupted by PN [6], [10]. The FP approach is an accurate way to provide such information.

The FP approach has been proposed by [1], [6], [8], [9], and [22]. They derived FP equations for a specified IF filter, the finite-time integrator. Using stochastic methods, we derive generalized equations for any IF filter with a bounded impulse response.

The IF filter part of a coherent receiver is shown in Fig. 1, where $s(t)$ is the input signal to the IF filter which is corrupted by PN, $h(t)$ is the impulse response of the IF filter, and $z(t)$ is

Paper approved by H. Leib, the Editor for Communication and Information Theory of the IEEE Communications Society. Manuscript received March 21, 2002; revised March 7, 2005. This work was supported by the National Science Foundation under grant NSF-RHA 0098382, "Diffusion Processes in Motion Planning and Control."

Y. Wang is with the Department of Mechanical Engineering, The College of New Jersey, Ewing, NJ 08628 USA (e-mail: jwang@tcnj.edu).

Y. Zhou is with the Department of Mechanical Engineering, State University of New York at Stony Brook, Stony Brook, NY 11794 USA (e-mail: yuzhou@notes.cc.sunysb.edu).

D. K. Maslen is with Susquehanna International Group, Bala Cynwyd, PA 19004 USA (e-mail: david@maslen.net).

G. S. Chirikjian is with the Department of Mechanical Engineering, Johns Hopkins University, Baltimore, MD 21218 USA (e-mail: gregc@jhu.edu).

Digital Object Identifier 10.1109/TCOMM.2006.873988

Fig. 1. IF part of a coherent receiver.

the output of the IF filter. Using the equivalent baseband representation and normalizing it to unit amplitude, the input signal can be written as [10]

$$s(t) = e^{j\phi(t)}$$

where $\phi(t)$ is the PN with zero mean and variance of Dt. The parameter D is the phase-diffusion coefficient, and related to the laser linewidth Δv by $D = 2\pi\Delta v$. $\phi(t)$ is usually modeled as a Brownian motion process [13]

$$\phi(t) = \sqrt{D}\int_0^t dW(\tau) \tag{1}$$

where $dW(t)$ is unit-strength white noise. The output of the IF filter, $z(t)$, is

$$z(t) = h(t) * s(t) = \int_0^t h(\tau)e^{j\phi(t-\tau)}d\tau. \tag{2}$$

Since PN $\phi(t)$ is a random process, the reversal of the time direction in $\phi(t)$ does not affect the statistics of $z(t)$. $\phi(t-\tau)$ can be replaced by $\phi(\tau)$. Equation (2) can be rewritten as

$$z(t) = \int_0^t h(\tau)e^{j\phi(\tau)}d\tau. \tag{3}$$

Let us expand $z(t)$ into its real $x(t)$ and imaginary $y(t)$ parts, or its magnitude $r(t)$ and phase $\theta(t)$ as

$$z(t) = x(t) + jy(t) = r(t)e^{j\theta(t)}. \tag{4}$$

From (3) and (4), we can get

$$x(t) = \int_0^t h(\tau)\cos\phi(\tau)d\tau \tag{5}$$

$$y(t) = \int_0^t h(\tau)\sin\phi(\tau)d\tau. \tag{6}$$

In the following, we will derive the stochastic differential equations (SDEs) first. Then we write the corresponding FP equations.

A. 3-D SDE

Though $z(t)$, $x(t)$, and $y(t)$ are not Markov processes, the three-component vector process, $[\phi(t), x(t), y(t)]^T$ is a Markov vector process. From (1), (5), and (6), we can derive the SDEs as

$$\begin{bmatrix} d\phi(t) \\ dx(t) \\ dy(t) \end{bmatrix} = \begin{bmatrix} 0 \\ h(t)\cos\phi(t) \\ h(t)\sin\phi(t) \end{bmatrix} dt + \begin{bmatrix} \sqrt{D} \\ 0 \\ 0 \end{bmatrix} dW(t) \tag{7}$$

with initial conditions $\phi(0) = 0$, $x(0) = 0$, $y(0) = 0$.

B. 2-D SDE

In many applications, the joint statistics of $x(t)$ and $y(t)$ [or, in polar coordinates, $r(t)$ and $\theta(t)$] are of interest. It is possible to suppress the $\phi(t)$ dimension in (7) by a slight modification of the process (3). Using a similar strategy as in [1], it can be shown that

$$dz(t) = h(t)dt - j\sqrt{D}z(t)dW(t). \tag{8}$$

Let us rewrite (8) in polar coordinates as the system of equations

$$\begin{bmatrix} dr(t) \\ d\theta(t) \end{bmatrix} \begin{bmatrix} h(t)\cos(\theta(t)) \\ -h(t)\sin(\theta(t))/r(t) \end{bmatrix} dt + \begin{bmatrix} 0 \\ -\sqrt{D} \end{bmatrix} dW. \tag{9}$$

C. Derivation of FP Equations

Consider a system with SDEs of the form

$$d\mathbf{X} = \mathbf{a}(\mathbf{X}(t), t)\,dt + H(\mathbf{X}(t), t)\,d\mathbf{W}(t) \tag{10}$$

where $\mathbf{X} \in \mathbb{R}^p$ and $\mathbf{W} \in \mathbb{R}^m$. $\mathbf{W}(t)$ is a Wiener process. Each component of $\mathbf{W}(t)$ has zero mean, are taken to be zero at time zero, and are stationary and independent processes. The notation $d\mathbf{W}(t)$ is defined by

$$d\mathbf{W}(t) = \mathbf{W}(t+dt) - \mathbf{W}(t).$$

Let $f(\mathbf{x}, t)$ be the PDF for $\mathbf{X}(t)$. The derivation of the FP equation governing the evolution of $f(\mathbf{x}, t)$ for a system of the form in (10) forced by a Wiener process can be obtained as in [2] and [3]

$$\frac{\partial f}{\partial t} = -\frac{1}{\sqrt{\det G}}\sum_{i=1}^{p}\frac{\partial}{\partial x_i}\left(\sqrt{\det G}a_i(x,t)f(x,t)\right) + \frac{1}{\sqrt{\det G}}\sum_{i,j=1}^{p}\frac{\partial^2}{\partial x_i \partial x_j}\left(\sqrt{\det G}(HH^T)_{ij}f(x,t)\right). \tag{11}$$

G is metric tensor with $\det G = 1$ for Cartesian coordinates and $\det G = r^2$ for polar coordinates.

1) 3-D FP Equation: Comparing (10) with (7), we see that

$$\mathbf{a} = \begin{bmatrix} 0 \\ h(t)\cos\phi(t) \\ h(t)\sin\phi(t) \end{bmatrix} \quad \text{and} \quad H\begin{bmatrix} \sqrt{D} \\ 0 \\ 0 \end{bmatrix}.$$

Using (11), we can derive the 3-D FP equation for (7) as

$$\frac{\partial f}{\partial t} = -h(t)\cos\phi\frac{\partial f}{\partial x} - h(t)\sin\phi\frac{\partial f}{\partial y} + \frac{D}{2}\frac{\partial^2 f}{\partial \phi^2} \tag{12}$$

with initial condition $f(x, y, \phi; 0) = \delta(x)\delta(y)\delta(\phi)$, δ being the Dirac delta function.

2) 2-D FP Equation: Comparing (10) with (9), we see that

$$\mathbf{a} = \begin{bmatrix} h(t)\cos(\theta(t))\,dt \\ -h(t)\sin(\theta(t))/r(t) \end{bmatrix}, \quad \mathbf{H} = \begin{bmatrix} 0 \\ -\sqrt{D} \end{bmatrix}$$

in polar coordinates.

The 2-D FP equations can then be derived using (10). They are explicitly written in polar coordinates as

$$\frac{\partial f}{\partial t} = -h(t)\cos\theta\frac{\partial f}{\partial r} + \frac{h(t)\sin\theta}{r}\frac{\partial f}{\partial \theta} + \frac{D}{2}\frac{\partial^2 f}{\partial \theta^2}. \tag{13}$$

The initial condition is $f(r, \theta; 0) = (1/r)\delta(r)\delta(\theta)$.

Equation (12) is the so-called 3-D PN FP equation, which has never been solved by other authors. It provides complete statistical information of the output of the IF filter. Equation (13) is the simplified 2-D PN FP equation. Solving these two equations for any type of IF filter in a general form is the main target of this paper. The involved mathematics will be introduced first in the next section.

III. Noncommutative Harmonic Analysis

Noncommutative harmonic analysis is a generalization of Fourier analysis for functions of group-valued argument. This mathematical tool was developed for the case of rigid-body motions by and for pure mathematicians and theoretical physicists in the 1960s [14]. It is rarely known by engineering scholars. In this paper, it is successfully applied to formulate and solve problems in the field of optical communications. This section introduces this powerful mathematical tool and some new results that we derived.

A. Euclidean Motion Group

The Euclidean motion group $SE(N)$ is the semidirect product of $\mathbb{R}^N$ with the special orthogonal group, $SO(N)$.[1] We denote elements of $SE(N)$ as $g = (\mathbf{a}, A) \in SE(N)$ where $A \in SO(N)$ and $\mathbf{a} \in \mathbb{R}^N$. For any $g = (\mathbf{a}, A)$ and $h = (\mathbf{r}, R) \in SE(N)$, the group law is written as $g \circ h = (\mathbf{a} + A\mathbf{r}, AR)$, and $g^{-1} = (-A^T\mathbf{a}, A^T)$.

It is often convenient to express an element of $SE(N)$ as a homogeneous transformation matrix of the form

$$g = \begin{pmatrix} A & \mathbf{a} \\ \mathbf{0}^T & 1 \end{pmatrix}.$$

[1]The group $SO(N)$ consists of $N \times N$ matrices with the properties $RR^T = I$ and $\det R = +1$. The group law is matrix multiplication.

For example, each element of $SE(2)$ parameterized using polar coordinates can be written as

$$g(r, \theta, \phi) = \begin{pmatrix} \cos\phi & -\sin\phi & r\cos\theta \\ \sin\phi & \cos\phi & r\sin\theta \\ 0 & 0 & 1 \end{pmatrix}$$

where $0 \le \phi, \theta \le 2\pi$, and $0 \le r \le \infty$. $SE(2)$ is a 3-D manifold much like $\mathbb{R}^3$. We can integrate over $SE(2)$ using the volume element $d(g(r, \theta, \phi)) = (1/4\pi^2) r dr d\theta d\phi$ [3].

B. Differential Operators Defined on the Motion Group

A function of motion takes elements of the motion group as its arguments. The partial derivatives of a function of motion $f(g)$ (or the differential operators acting on functions on the motion group) are defined as [14]

$$\tilde{X}_i^R f \triangleq \frac{d}{dt} f\left(g \circ \exp(t\tilde{X}_i)\right)\Big|_{t=0}$$
$$\tilde{X}_i^L f \triangleq \frac{d}{dt} f\left(\exp(-t\tilde{X}_i) \circ g\right)\Big|_{t=0}.$$

Here $\tilde{X}_i$ is the ith natural basis element for the Lie algebra associated with a motion group. For the case of $SE(2)$

$$\tilde{X}_1 = \begin{pmatrix} 0 & -1 & 0 \\ 1 & 0 & 0 \\ 0 & 0 & 0 \end{pmatrix}$$
$$\tilde{X}_2 = \begin{pmatrix} 0 & 0 & 1 \\ 0 & 0 & 0 \\ 0 & 0 & 0 \end{pmatrix}$$
$$\tilde{X}_3 = \begin{pmatrix} 0 & 0 & 0 \\ 0 & 0 & 1 \\ 0 & 0 & 0 \end{pmatrix}.$$

For small values of t, the infinitesimal motion $\exp(t\tilde{X}_i)$ is the matrix exponential function. In our notation, the superscripts R and L denote whether the infinitesimal motion $\exp(t\tilde{X}_i)$ is on the right or the left of g. Hence, $\tilde{X}_i^R$ is invariant under left shifts, and $\tilde{X}_i^L$ is invariant under right shifts. Explicitly, we can derive the differential operators $\tilde{X}_i^R$ in polar coordinates as [21]

$$\tilde{X}_1^R = \frac{\partial}{\partial \phi} \tag{14}$$

$$\tilde{X}_2^R = \cos(\phi - \theta)\frac{\partial}{\partial r} + \frac{\sin(\phi - \theta)}{r}\frac{\partial}{\partial \theta} \tag{15}$$

$$\tilde{X}_3^R = -\sin(\phi - \theta)\frac{\partial}{\partial r} + \frac{\cos(\phi - \theta)}{r}\frac{\partial}{\partial \theta} \tag{16}$$

and in Cartesian coordinates as

$$\tilde{X}_1^R = \frac{\partial}{\partial \phi} \tag{17}$$

$$\tilde{X}_2^R = \cos\phi\frac{\partial}{\partial x} + \sin\phi\frac{\partial}{\partial y} \tag{18}$$

$$\tilde{X}_3^R = -\sin\phi\frac{\partial}{\partial x} + \cos\phi\frac{\partial}{\partial y}. \tag{19}$$

The differential operators $\tilde{X}_i^L$ in polar coordinates are

$$\tilde{X}_1^L = -\frac{\partial}{\partial\phi} - \frac{\partial}{\partial\theta} \tag{20}$$

$$\tilde{X}_2^L = -\cos\theta\frac{\partial}{\partial r} + \frac{\sin\theta}{r}\frac{\partial}{\partial\theta} \tag{21}$$

$$\tilde{X}_3^L = -\sin\theta\frac{\partial}{\partial r} - \frac{\cos\theta}{r}\frac{\partial}{\partial\theta}. \tag{22}$$

C. Motion-Group Fourier Transform

The Fourier transform of a function of motion $f(g)$ is an infinite-dimensional matrix defined as [3]

$$\mathcal{F}(f) = \hat{f}(p) = \int_G f(g)U(g^{-1},p)d(g)$$

where $d(g)$ is a volume element at g, and $U(g,p)$ is an infinite-dimensional matrix function of g and a "frequency" parameter p. The corresponding inverse Fourier transform (IFT) is

$$f(g) = \mathcal{F}^{-1}(f) = \int_{\hat{G}} \text{trace}\left[\hat{f}(p)U(g,p)\right] d\nu(p)$$

where $\hat{G}$ is the space of all p values called the dual of the group G, and ν is an appropriately chosen integration measure in a generalized sense on $\hat{G}$.

For the case of $SE(2)$, the matrix elements of $U(g,p)$ are expressed explicitly as [3]

$$u_{mn}\left(g(r,\theta,\phi),p\right) = j^{n-m}e^{-j[n\phi+(m-n)\theta]}J_{n-m}(pr) \tag{23}$$

where $J_k(x)$ is the kth-order Bessel function. The IFT can be written in terms of elements as

$$f(g) = \sum_{m,n\in\mathsf{Z}}\int_0^\infty \hat{f}_{mn}u_{nm}(g,p)pdp. \tag{24}$$

D. Operational Properties

In analogy with the classical Fourier transform, which converts derivatives of functions of position into algebraic operations in Fourier space, there are operational properties for the motion-group Fourier transform (MGFT).

By the definition of the the MGFT $\mathcal{F}$ and differential operators $\tilde{X}_i^R$ and $\tilde{X}_i^L$, we can derive the Fourier transform of the derivatives of a function of motion as [3]

$$\begin{aligned}\mathcal{F}\left[\tilde{X}_i^R f\right] &= \eta(X_i,p)\hat{f}(p)\\ \mathcal{F}\left[\tilde{X}_i^L f\right] &= -\hat{f}(p)\eta(X_i,p)\end{aligned} \tag{25}$$

where

$$\eta(X_i,p) \triangleq \frac{d}{dt}\left(U\left(\exp(tX_i),p\right)\right)\big|_{t=0}.$$

The explicit expression of $\eta(\tilde{X}_i,p)$ for $SE(2)$ can be derived as follows.

The matrix elements of $U(\exp(t\tilde{X}_1),p)$ can be obtained from (23) by setting $\phi = t$, $r = 0$, and $\theta = 0$

$$u_{mn}\left(\exp(t\tilde{X}_1),p\right) = e^{-jmt}\delta_{m,n}.$$

The fact that

$$J_{m-n}(0) = \begin{cases}1, & \text{for } m-n=0\\ 0, & \text{for } m-n\neq 0\end{cases}$$

is used in the above calculation. It then follows that

$$\eta_{mn}(\tilde{X}_1,p) = -jm\delta_{m,n}. \tag{26}$$

The matrix elements of $U(\exp(t\tilde{X}_2),p)$ can be obtained from (23) by setting $\phi = 0$, $r = t$, and $\theta = 0$

$$u_{mn}\left(\exp(t\tilde{X}_2),p\right) = j^{n-m}J_{n-m}(pt).$$

It is known that

$$\frac{d}{dx}J_m(x) = \frac{1}{2}\left[J_{m-1}(x) - J_{m+1}(x)\right].$$

Hence

$$\eta_{mn}(\tilde{X}_2,p) = \frac{jp}{2}(\delta_{m,n+1} + \delta_{m,n-1}). \tag{27}$$

The matrix elements of $U(\exp(t\tilde{X}_3),p)$ can be obtained from (23) by setting $\phi = 0$, $r = t$, $\theta = \pi/2$

$$u_{mn}\left(\exp(t\tilde{X}_3),p\right) = (-1)^{n-m}J_{n-m}(pt)$$

and so

$$\eta_{mn}(\tilde{X}_3,p) = \frac{p}{2}(\delta_{m,n+1} - \delta_{m,n-1}). \tag{28}$$

IV. Solutions to Fokker–Planck Equations

The general procedure to solve FP equations is as follows.

Step 1) Restate the FP equation using the differential operators defined on the motion group.

Step 2) Apply the MGFT to convert the equation into a system of linear ODEs.

Step 3) Solve these ODEs.

Step 4) Recover the PDF of the filtered signal using the inverse MGFT.

A. Solutions to the 3-D FP (12)

Using differential operators given in (17) and (18), the 3-D FP (12) can be rewritten as

$$\frac{\partial f}{\partial t} = \left(-h(t)\tilde{X}_2^R + \frac{D}{2}\left(\tilde{X}_1^R\right)^2\right) f. \tag{29}$$

Applying the MGFT to (29) and using the result of (25), we can convert it to an infinite system of linear ODEs

$$\frac{d\hat{f}}{dt} = C_1\hat{f} \tag{30}$$

where the coefficient matrix C_1 is

$$C_1 = -h(t)\eta(\tilde{X}_2, p) + \frac{D}{2}\left[\eta(\tilde{X}_1, p)\right]^2.$$

The explicit expressions for the above $\eta(\tilde{X}_i, p)$ have been derived in (26) and (27). The elements of the matrix C_1 can be written explicitly as

$$C_{1,mn} = -h(t)\frac{jp}{2}(\delta_{m,n+1} + \delta_{m,n-1}) - \frac{D}{2}m^2\delta_{m,n}.$$

Once we get the solution to the ODE (30), we can then substitute it into the Fourier inversion formula (24) for the motion group to recover the PDF $f(g(r,\theta,\phi);t)$ of $z(t)$. To get the joint PDF $f(r,\theta;t)$ is just an integration, with respect to ϕ, as

$$\begin{aligned} f(r,\theta;t) &= \frac{1}{2\pi}\int_0^{2\pi} f(g;t)d\phi \\ &= \sum_{n\in Z} j^{-n}e^{-jn\theta}\int_0^{\infty}\hat{f}_{0,n}J_{-n}(pr)pdp. \end{aligned} \tag{31}$$

Integrating (31) over θ will give us the marginal PDF $|z(t)|$ of $z(t)$ as

$$|z(t)| = f(r;t) = \int_0^{\infty}\hat{f}_{0,0}(p)J_0(pr)pdp. \tag{32}$$

Equation (32) gives us a simple and compact expression for the marginal PDF for the output of the IF filter.

B. Solutions to the 2-D FP (13)

Using differential operators given in (14), (20), and (21), the 2-D FP (13) can be rewritten as

$$\frac{\partial f}{\partial t} = \left(h(t)\tilde{X}_2^L + \frac{D}{2}\left(\tilde{X}_1^R + \tilde{X}_1^L\right)^2\right) f. \tag{33}$$

Applying the MGFT to (33) and using the result of (25), we can convert them to an infinite system of linear ODEs

$$\frac{d\hat{f}}{dt} = \hat{f}C_2 + C_3\hat{f} - C_4\hat{f}C_4 \tag{34}$$

where the matrices C_2, C_3, and C_4 are

$$\begin{aligned} C_2 &= -h(t)\eta(\tilde{X}_2, p) + \frac{D}{2}\left[\eta(\tilde{X}_1, p)\right]^2 \\ C_3 &= \frac{D}{2}\left[\eta(\tilde{X}_1, p)\right]^2 \\ C_4 &= \sqrt{D}\eta(\tilde{X}_1, p). \end{aligned}$$

The explicit expressions for the above $\eta(\tilde{X}_i, p)$ have been derived in (26) and (27).

Though numerical methods can be applied to solve (34), we can further simplify (34) to the simplest format as [21]

$$\frac{d\hat{\mathbf{F}}_0}{dt} = C_5^T\hat{\mathbf{F}}_0 \tag{35}$$

where $\hat{\mathbf{F}}_0 = [\hat{f}_{0,-m}, \cdots, \hat{f}_{0,0}, \cdots, \hat{f}_{0,m}]^T$. The elements of C_5 are of the form

$$C_{5,mn} = -h(t)\frac{jp}{2}(\delta_{m,n+1} + \delta_{m,n-1}) - \frac{D}{2}m^2\delta_{m,n}.$$

The reader may notice that the coefficient matrices C_1 and C_5 are the same. Substituting the solution to (35) into the motion-group Fourier inversion formula (24), we can obtain the PDF $f(g;t)$ of $z(t)$. Equations (31) and (32) can then be used to get the joint PDF $f(r,\theta;t)$ and the marginal PDF $|z(t)|$ of $z(t)$, respectively.

V. Numerical Results

For comparison, we first generate some results for a finite-time integrator which has a bounded time response

$$h(t) = \begin{cases} 1, & 0 \le t \le \tau \le T \\ 0, & \text{otherwise} \end{cases} \tag{36}$$

where T is the bit duration. This is the case that has been addressed by other authors.

We can get the PDF of the filtered signal by solving either the 3-D FP equation or the 2-D FP equation. There is no difference in the computational procedure when using our method. However, no other works in the literature have solved the 3-D FP equation, so far.

Three situations are illustrated. They are expressed in terms of the value of Dt. Dt reflects the amount of PN. It is the variance of PN over the integration time t of the IF filter. Increasing Dt implies an increase in PN. A small value of Dt can be obtained either by reducing the laser linewidth Δv, or by decreasing the integration time t. The 3-D FP (12) is used for $Dt = 6$, and the 2-D FP (13) is used for $Dt = 1$ and $Dt = 8$.

For the finite-time integrator, the coefficient matrix C_1 of ODE (30) corresponding to the 3-D FP equation becomes a constant matrix whose m,n-element is

$$C_{1,mn} = -\frac{jp}{2}(\delta_{m,n+1} + \delta_{m,n-1}) - \frac{D}{2}m^2\delta_{m,n}.$$

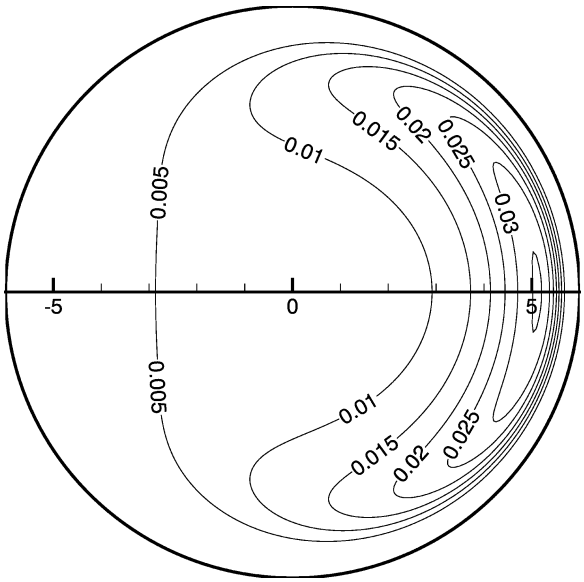

Fig. 2. Contour plot of the joint PDF, $f(r, \theta; t)$, using the 3-D FP equation with $Dt = 6$.

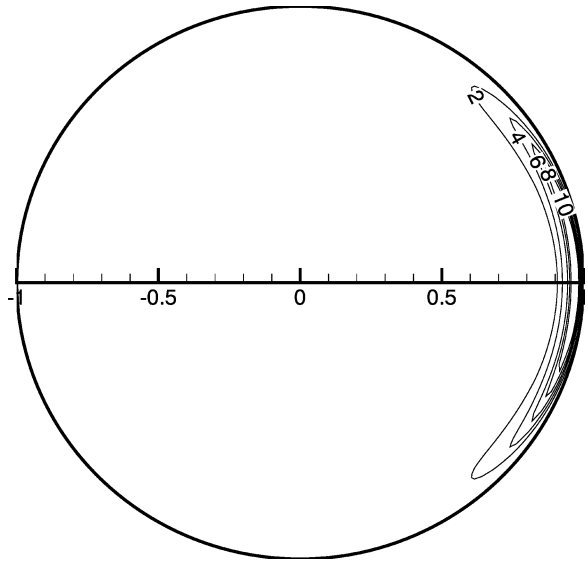

Fig. 3. Contour plot of the joint PDF, $f(r, \theta; t)$, using the 2-D FP equation with $Dt = 1$.

In this case, ODE (30) is a simple linear time-invariant system. It can be easily solved, subject to the given initial conditions by matrix exponential as

$$\hat{f}(p; t) = \exp(C_1 t). \tag{37}$$

The joint and marginal PDF of $z(t)$ can then be obtained by substituting (37) into (31) and (32), respectively. Fig. 2 shows the contour plot of the joint PDF of $z(t)$ with $Dt = 6$.

Similarly, the coefficient matrix C_5 of ODE (35) corresponding to the 2-D FP equation becomes a constant matrix whose m, n-element is

$$C_{5,mn} = -\frac{jp}{2}(\delta_{m,n+1} + \delta_{m,n-1}) - \frac{D}{2} m^2 \delta_{m,n}.$$

By matrix exponential, we can get the solution to this ODE. Using (31) and (32), we can get the joint PDF and the marginal PDF. Figs. 3 and 4 show the contour plots of the joint PDF of $z(t)$ for Dt having the values 1 and 8. Fig. 5 shows the marginal PDF of $z(t)$ for different amounts of PN, indicated by the values of Dt. These plots are the same as those given by [10]. These identical results verify our proposed computational method.

Using our method, we can also easily obtain the results for the time-varying filters which other methods have difficulty in solving. In these cases, our method converts FP equations into time-varying linear ODEs. For illustration, we apply our method to a raised cosine filter and an RC filter. Since the time-normalized axis is usually adopted by other authors in considering filter impulse responses of different shapes, we use the time-normalized impulse responses as given in [7] and [12]. Whether the time axis is normalized or not will not affect the effectiveness

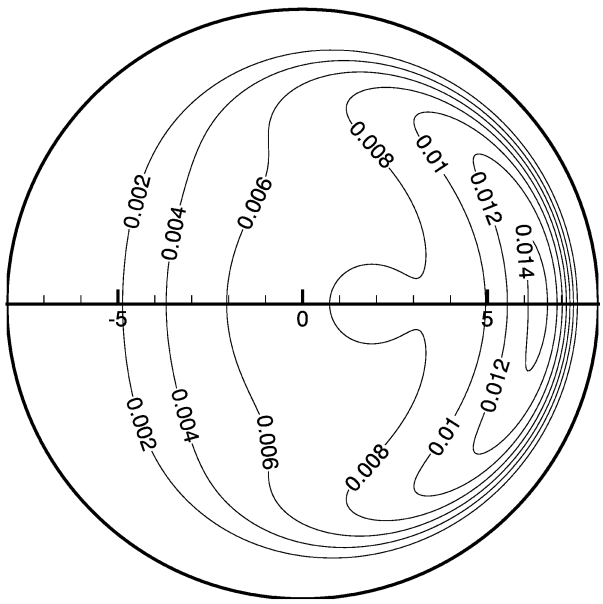

Fig. 4. Contour plot of the joint PDF, $f(r, \theta; t)$, using the 2-D FP equation with $Dt = 8$

of our method. The impulse response of the raised cosine filter is defined as [12]

$$h(t) = \begin{cases} 1 - \cos 2\pi t, & 0 \le t \le 1 \\ 0, & \text{otherwise} \end{cases} \tag{38}$$

and the impulse response of the RC filter [7] is

$$h(t) = \begin{cases} 4e^{-4t}, & 0 \le t \le 1 \\ 0, & \text{otherwise.} \end{cases} \tag{39}$$

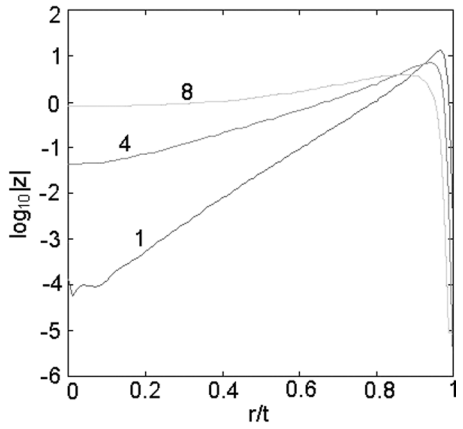

Fig. 5. Marginal PDF $|z|$ for different values of Dt.

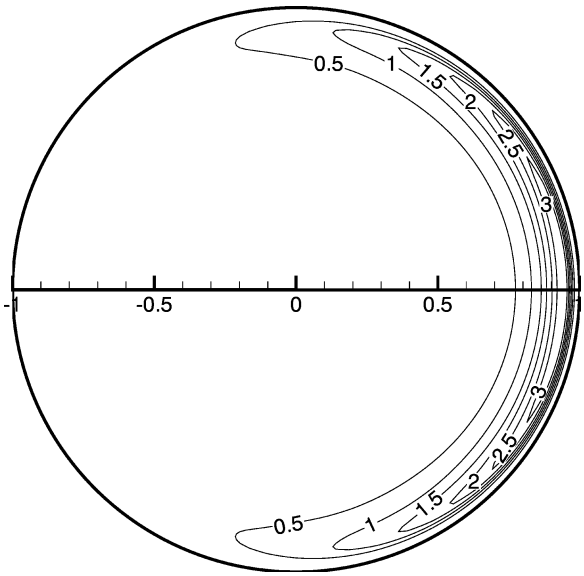

Fig. 6. Contour plot of the joint PDF for a raised cosine filter with $Dt = 3$.

There is no big difference for applying our method to either the 3-D FP equation or the 2-D FP equation. Here, we use (12) for the raised cosine filter and (13) for the RC filter.

For the raised cosine filter, the coefficient matrix C_1 of ODE (30) corresponding to the 3-D FP equation is a time-varying matrix whose mnth element is

$$C_{1,mn} = -(1 - \cos 2\pi t)\frac{jp}{2}(\delta_{m,n+1} + \delta_{m,n-1}) - \frac{D}{2}m^2\delta_{m,n}.$$

For the RC filter, the coefficient matrix C_5 of ODE (35) corresponding to the 2-D FP equation is a time-varying matrix whose mnth element is

$$C_{5,mn} = -(4e^{-4t})\frac{jp}{2}(\delta_{m,n+1} + \delta_{m,n-1}) - \frac{D}{2}m^2\delta_{m,n}.$$

Runge–Kutta integration can be used to solve this simple linear time-variant system. Figs. 6 and 7 show the contour plots of the joint PDF of $z(t)$ for the raised cosine filter and the RC filter with $Dt = 3$, respectively.

The application and interpretation of these PDFs have been well addressed in [5]–[8], [10], and [12]. In these papers, these PDFs have been used to study the optimum threshold setting,

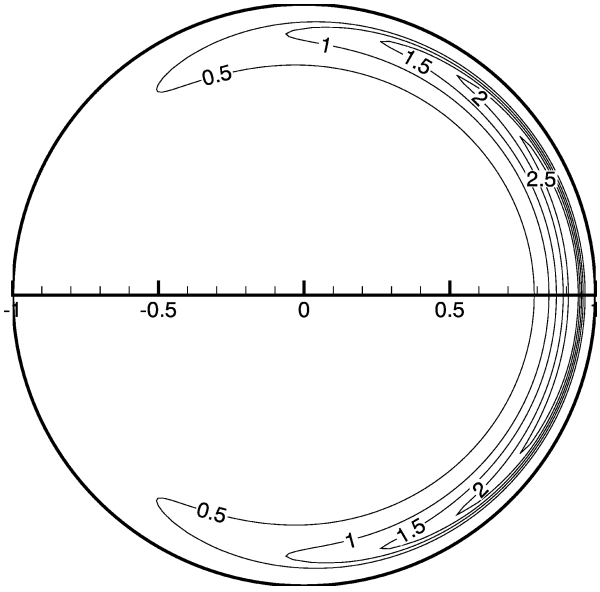

Fig. 7. Contour plot of the joint PDF for an RC filter with $Dt = 3$.

TABLE I
TRUNCATION LIMIT

	p_B	L_{B1}	L_{B2}
Dt=1 (Figures 2 and 5)	1200	20	4
Dt=8 (Figures 3 and 8)	800	12	4
Dt=6 (Figure 4)	800	12	4
Dt=4 (Figure 5)	800	12	4
Dt=3 (Figures 6 and 7)	800	12	4

bit rate error, IF bandwidth, detection strategies, and receiver performance for coherent optical communication systems. We will not discuss this aspect here, due to the main goal of this paper and page limits.

For the above computations, the infinite-dimensional matrix function $U(g,p)$ in the Fourier transform is truncated. The bandlimited approximation still gives us very accurate results, because the magnitude of the Fourier transform of a function can be ignored beyond a certain cutoff frequency. The upper bound of the frequency parameter p is chosen to be P_B rather than infinity when performing integration in p. The dimension of the truncated $U(g,p)$ is chosen to be $2L_{B1} + 1$ for the forward Fourier transform and $2L_{B2} + 1$ for the IFT. Values of L_{B1} and L_{B2} are listed in Table I. The truncation of $U(g,p)$ potentially makes the outer elements (values of $\hat{f}$ with $|m|, |n| \to L_{B1}$) have errors. This is why we impose a second truncation on $U(g,p)$ of L_{B2} when substituting into the Fourier inverse formula. For small amounts of PN, we need larger values of L_{B1} and p_B. If p_B is not large enough, it will cause Gibbs-like oscillations in the marginal PDF near the origin.

VI. COMPARISON WITH OTHER METHODS

While the purpose of this paper is to introduce the method of noncommutative harmonic analysis (i.e., Fourier transform on $SE(2)$) to solve the PN FP equations, a comparison between the results obtained by using this method and those obtained from existing statistical methods provides a basis for comparison in the evaluation of the performance of the proposed method.

As discussed in the previous section, the instantaneous state of the system, denoted as $\mathbf{x}(t) = [d\phi(t), dx(t), dy(t)]$, is a random variable at time t. This paper's interest is in estimating the time evolving PDF of $\mathbf{x}(t)$, denoted as $f(\mathbf{x}, t)$. Besides the category of analytical methods such as the one proposed in this paper, the category of data-driven methods has been widely used in density estimation [4], [16], [17]. In our case, "data-driven" can be understood as generating a PDF of a random variable from a set of its sample values, which is a set of possible values of $\mathbf{x}$ at time t in the context of this paper. Among the most accepted methods to generate smooth and continuous PDFs are the kernel-density estimation methods [4], [16], [17]. Let $\mathbf{X}$ be an n by d matrix of random vectors $\mathbf{x}_i = (x_{i1}, \ldots, x_{id})$, where $\mathbf{x}_1, \ldots, \mathbf{x}_n$ are independent samples from a PDF $f(\mathbf{x})$ of dimension d. Let $\mathbf{x}$ be a vector of dimension d. The kernel estimator of $f(\mathbf{x})$ is given by

$$\tilde{f}(\mathbf{x}) = \frac{1}{n}\sum_{i=1}^{n}\prod_{j=1}^{d}\frac{1}{h_j}K\left(\frac{x_j - X_{ij}}{h_j}\right) \tag{40}$$

where x_j is the jth component of $\mathbf{x}$, X_{ij} is the ijth entry of $\mathbf{X}$, K is the same 1-D kernel function used in each dimension, and h_j is the smoothing parameter for the jth dimension. In addition, the methods to select optimal smoothing parameters for kernel-density estimation have been studied, among which the bootstrap method, the least-squares (LS) (unbiased) cross-validation method, and the biased cross-validation method are widely used [15]–[17], [20].

To estimate $f(\mathbf{x}, t)$ by using a data-driven density-estimation method, a set of sample values of $\mathbf{x}$ at time t need to be generated. Recently, a Monte Carlo approach, the Euler–Maruyama method, was introduced and explained in detail by Higham as a numerical method for SDEs [11]. The SDE under current discussion is given as (7), with initial conditions $\phi(0) = 0$, $x(0) = 0$, $y(0) = 0$. With the Euler–Maruyama method, a sample value of $\mathbf{x}$ at time t can be calculated by doing numerical integration to (7), along a discretized Brownian path in the following form:

$$\mathbf{x}(t) = \mathbf{x}(0) + \int_0^t \mathbf{a}(\mathbf{x}(\tau))\, d\tau + \int_0^t \mathbf{H}(\mathbf{x}(\tau))\, d\mathbf{W}(\tau) \tag{41}$$

where $\mathbf{x} = [d\phi, dx, dy]^T$, $\mathbf{a} = [0, h(t)\cos\phi(t), h(t)\sin\phi(t)]^T$, $\mathbf{H} = [\sqrt{D}, 0, 0]^T$, $\mathbf{W}$ denotes a Wiener process, and $d\mathbf{W}(t) = \mathbf{W}(t + dt) - \mathbf{W}(t)$. In this way, a number of sample values of $\mathbf{x}$ at time t can be calculated from a number of discretized Brownian paths which are generated with a random number generator. Then the desired PDF can be estimated by using the method described in the last paragraph.

In the following, we use the method of Gaussian kernel-density estimation together with the Euler–Maruyama method to estimate $f(\mathbf{x}, t)$. Then we compare the resulting $f(\mathbf{x}, t)$ with the ones obtained from the method of the Fourier transform on $SE(2)$. The whole procedure consists of the following steps.

1) Use the Euler–Maruyama method to generate a set of reachable values of $\mathbf{x}$ at time t by performing the integrals in (41).
2) Search for the optimal smoothing parameters for Gaussian kernel-density estimation by using the LS cross-validation method. The smoothing parameters are indeed the standard deviations along all Cartesian and rotational axes.
3) Use the Gaussian kernel-density estimation method to evaluate $f(\mathbf{x}, t)$.
4) Root mean square (RMS) error of the resulting $f(\mathbf{x}, t)$ is calculated, and the time taken to finish steps 1–3 is recorded.
5) Repeat steps 1–3 with different numbers of sample values of $\mathbf{x}$, and record a set of values of RMS error and corresponding computation time. We plot the RMS error of the data-driven method as a function of computation time.
6) Compare the resulting curve with the one obtained from the method of the Fourier transform on $SE(2)$, which is discussed in detail in previous sections.

One may notice that we use the LS cross-validation method to search for the optimal smoothing parameters. The choice is based on the test of all three methods mentioned above, i.e., the bootstrap, the LS cross-validation, and the biased cross-validation. For the PN problem described by (7), when Dt is large enough, the Gaussian kernel-density estimation can generate smooth PDFs with the optimal smoothing parameters obtained from all three optimization methods. However, when Dt is small, such as $Dt = 1$, the resulting PDFs with the smoothing parameters obtained from the bootstrap and the biased cross-validation methods are over-smoothed, and, as a result, cannot show the "crescent shape" feature (Fig. 3). As we tested, in the case of this PN problem, only the LS cross-validation method works stably at any time t, given a constant D. Therefore, we choose the LS cross-validation method to do the optimal smoothing parameter searching.

As a data-driven method, with a chosen automatic searching method for optimal smoothing parameters, the precision of the Gaussian kernel-density estimation completely depends on the number of samples. With the Euler–Maruyama method, the time to generate the set of sample values of $\mathbf{x}$ increases linearly with respect to the number of values. As we tested, the searching process of the optimal smoothing parameters consumes most of the total computation time. Moreover, it increases nearly quadratically with respect to the number of sample values, and therefore, as a result, it occupies a larger portion of the overall computation time.

On the other side, since the Fourier transform on the $SE(2)$ method deals with the infinite domain of p and infinite-dimensional Fourier matrices in principle, it is necessary to truncate them to the finite domain of p and the finite-dimensional matrices, so that it can be implemented numerically. In addition, the infinitesimal dp in the involved integration must be replaced by the finite increment Δp. Therefore, the precision of the Fourier transform on the $SE(2)$ method depends on the truncated matrix width, the upper bound of p, and the step in p. These factors also determine the time complexity of this method.

Based on the above analysis, we compare both methods under the same conditions. First, following the discussion in previous sections, we compute the joint PDF $f(r, \theta; t)$. Second, to set a reasonable time frame for comparison, we choose $Dt = 8$. In general, as Dt increases, the required computation time for the

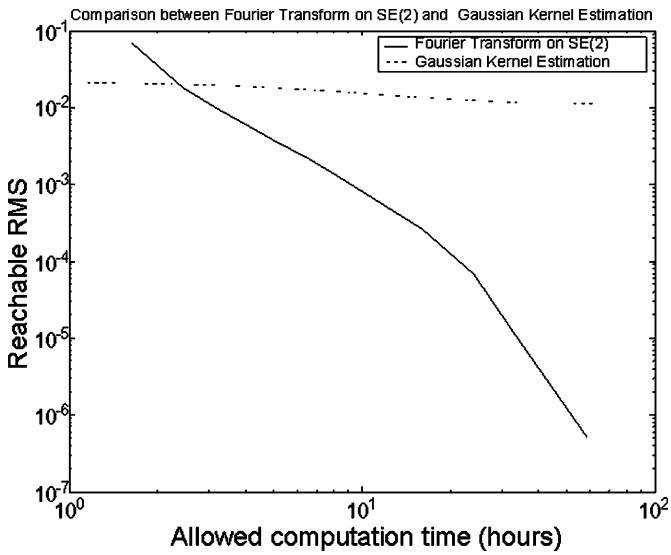

Fig. 8. Comparison between the Fourier transform on $SE(2)$ and the Gaussian kernel-density estimation.

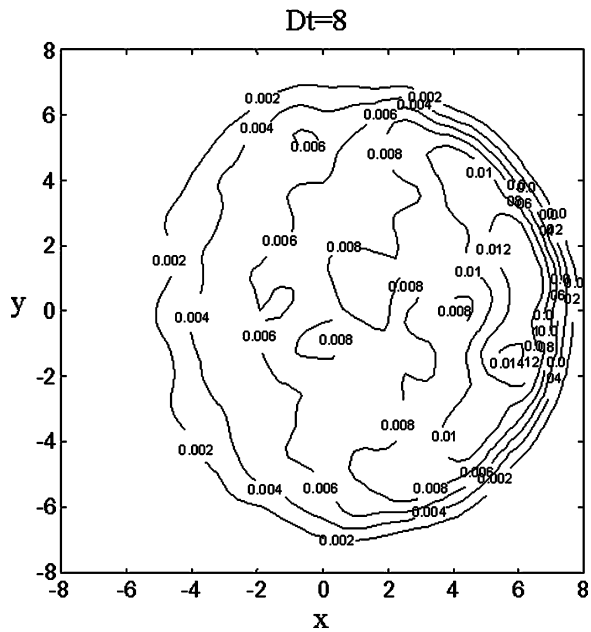

Fig. 9. PDF generated by Gaussian kernel-density estimation with the smoothing parameters chosen by the LS cross-validation (8000 samples, about 51 hours).

data-driven density-estimation method increases, while the time for the method of the Fourier transform on $SE(2)$ decreases, because a truncated matrix with a relatively small width can be used. Third, we limit the computation to 50×50 points on the PDF surface. Clearly, different numbers of surface points require different computation times. While the number of the surface points will not cause much difference when using the data-driven density estimation, the computation time of the method of the Fourier transform on $SE(2)$ is proportional to it. All of the computation is done on a Pentium 4 2-GHz Desktop PC. Under these equal conditions, we followed the above steps and did a series of computations. The comparison between the two methods is shown in Fig. 8. In the plot, the horizontal axis is the allowed computation time, and the vertical axis is the reachable RMS error of the resulting PDF. Therefore, the plot in fact shows the relationship between the reachable precision of both methods and the allowed computation time. Clearly, as the allowed computation time increases, the precision of both methods can be improved monotonically, but the method of the Fourier transform on $SE(2)$ shows a much quicker rate of improvement. As one can see, there is a breakeven at a small time limit. The reason is that for a small time limit, the computation can be implemented by the kernel method with a small number of samples, and the cross-validation method can adjust the smoothing parameters to provide an optimal PDF. Meanwhile, the computation can only be realized by the Fourier transform on the $SE(2)$ method with a small domain of p or a large Δp, which impairs the precision of the results for small values of Dt. In practice, with a reasonable time limit, a certain large domain of p and a certain small Δp are always used. Therefore, we can conclude that with a reasonable time limit, the Fourier transform on $SE(2)$ provides a more accurate density estimation than the Gaussian kernel-density estimation method.

Meanwhile, as another comparison in the quality of the resulting PDF, one can see that the PDF generated by the Fourier transform on the $SE(2)$ method (Fig. 4) is much smoother than the one generated by the Gaussian kernel-density estimation method with the smoothing parameters chosen by LS cross-validation (Fig. 9).

VII. Conclusion

In this paper, we have derived generalized FP equations from stochastic processes and shown that concepts from noncommutative harmonic analysis are useful in the numerical solution of these equations that arise in the analysis of PN in coherent optical communication systems. In particular, we used the operational properties of the MGFT to transform these FP equations into a system of linear ODEs in a generalized Fourier space. These ODEs are solvable by matrix exponentiation or Runge–Kutta integration, depending on the type of IF filters. The straightforward solution of these equations leads to a systematic method for solving the original equation of interest. Since this new computational method removes the computational difficulty which previously existed in solving the PN FP equations, we hope that the FP approach can become a more widely used design and analysis tool in coherent optical communication systems.

References

[1] D. J. Bond, "The statistical properties of phase noise," *Br. Telecommun. Tech. J.*, vol. 7, no. 4, pp. 12–17, Oct. 1989.

[2] R. Brockett, "Notes on stochastic processes on manifolds," in *Systems and Control in the Twenty-First Century*. Boston, MA: Birkhauser, 1997.

[3] G. S. Chirikjian and A. B. Kyatkin, *Engineering Applications of Noncommutative Harmonic Analysis*. Boca Raton, FL: CRC Press, 2000.

[4] L. Devroye, *A Course in Density Estimation*. Boston, MA: Birkhauser, 1987.

[5] G. J. Foschini, L. J. Greenstein, and G. Vannucci, "Noncoherent detection of coherent lightwave signals corrupted by phase noise," *IEEE Trans. Commun.*, vol. 36, no. 3, pp. 306–314, Mar. 1988.

[6] G. J. Foschini and G. Vannucci, "Characterizing filtered light waves corrupted by phase noise," *IEEE Trans. Inf. Theory*, vol. 34, no. 6, pp. 1437–1448, Nov. 1988.

[7] G. J. Foschini, G. Vannucci, and L. J. Greenstein, "Envelope statistics for filtered optical signals corrupted by phase noise," *IEEE Trans. Commun.*, vol. 37, no. 12, pp. 1293–1302, Dec. 1989.
[8] I. Garrett and G. Jacobsen, "Possibilities for coherent optical communication systems using lasers with large phase noise," *Br. Telecommun. Tech. J.*, vol. 7, no. 4, pp. 5–11, Oct. 1989.
[9] ——, "Phase noise in weakly coherent systems," *Proc. IEEE*, vol. 136, pt. J, pp. 159–165, Jun. 1989.
[10] I. Garrett, D. J. Bond, J. B. Waite, D. S. L. Lettis, and G. Jacobsen, "Impact of phase noise in weakly coherent systems: A new and accurate approach," *J. Lightw. Technol.*, vol. 8, no. 3, pp. 329–337, Mar. 1990.
[11] D. J. Higham, "An algorithmic introduction to numerical simulation of stochastic differential equations," *SIAM Rev.*, vol. 43, no. 3, pp. 525–546, Sep. 2001.
[12] G. Jacobsen, *Noise in Digital Optical Transmission Systems*. Norwood, MA: Artech House, 1994.
[13] L. Kazovsky, S. Benedetto, and A. Willner, *Optical Fiber Communication Systems*. Norwood, MA: Artech House, 1996.
[14] W. Miller, *Lie Theory and Special Functions*. New York: Academic, 1968.
[15] S. R. Sain, K. A. Baggerly, and D. W. Scott, "Cross-validation of multivariate densities," *J. Am. Statist. Assoc.*, vol. 89, no. 427, pp. 807–817.
[16] D. W. Scott, *Multivariate Density Estimation*. New York: Wiley, 1992.
[17] B. W. Silverman, *Density Estimation for Statistics and Data Analysis*. London, U.K.: Chapman & Hall, 1986.
[18] M. Stefanovic and D. Milic, "An approximation of filtered signal envelope with phase noise in coherent optical systems," *J. Lightw. Technol.*, vol. 19, no. 11, pp. 1685–1690, Nov. 2001.
[19] J. B. Waite and D. S. L. Lettis, "Calculation of the properties of phase noise in coherent optical receivers," *Br. Telecommun. Tech. J.*, vol. 7, no. 4, pp. 18–26, Oct. 1989.
[20] M. P. Wang and M. C. Jones, *Kernel Smoothing*. London, U.K.: Chapman & Hall, 1995.
[21] Y. F. Wang, "Applications of diffusion processes in robotics, optical communications and polymer science," Ph.D. dissertation, Johns Hopkins Univ., Baltimore, MD, 2001.
[22] X. Zhang, "Analytically solving the Fokker-Planck equation for the statistical characterization of the phase noise in envelope detection," *J. Lightw. Technol.*, vol. 13, no. 8, pp. 1787–1794, Aug. 1995.

Yunfeng Wang (M'04) received the B.S. and M.S. degrees in mechanical engineering from Tianjin University, Tianjin, China, in 1992 and 1995, respectively, and the M.S.E. degree in electrical and computer engineering in 2001, and the Ph.D. degree in mechanical engineering in 2002, both from Johns Hopkins University, Baltimore, MD.

Dr. Wang is currently an Assistant Professor in the Department of Mechanical Engineering, The College of New Jersey, Ewing, NJ. Her research interests include manipulator kinematics and dynamics, computational methods, autonomous vehicles, and intelligent manufacturing.

Yu Zhou (M'06) received the B.S. and M.S. degrees from Nanjing University of Aeronautics and Astronautics, Nanjing, China, and the Ph.D. degree from Johns Hopkins University, Baltimore, MD, in 2004, all in mechanical engineering.

He is currently an Assistant Professor in the Department of Mechanical Engineering, State University of New York at Stony Brook, Stony Brook, NY. His research interests include robot dynamics and kinematics, motion planning, stochastic modeling of mechanical systems with uncertainty, and macromolecular mechanics.

David Keith Maslen received the B.Sc. degree from the University of Otago, Dunedin, New Zealand, and the Ph.D. degree from Harvard University, Cambridge, MA, both in mathematics.

He has previously held positions at the Max-Planck-Institut für Mathematik, Universiteit Utrecht, Centrum voor Wiskunde en Informatica, and Dartmouth College. He is currently a Quantitative Research Associate with the Susquehanna International Group, Bala Cynwyd, PA. His interests include representation theory, computational harmonic analysis, and mathematical finance.

Gregory S. Chirikjian (M'03) was born August 16, 1966 in New Brunswick, NJ. He received the B.S.E. degree in engineering mechanics, the M.S.E. degree in mechanical engineering, and the B.A. degree in mathematics, all from The Johns Hopkins University, Baltimore, MD, in 1988. He then received the Ph.D. degree from the California Institute of Technology, Pasadena, CA, in 1992.

Since 1992, he has been on the faculty of the Department of Mechanical Engineering, Johns Hopkins University, where he is now a Professor. His research interests include the kinematic analysis, motion planning, design, and implementation of hyper-redundant, metamorphic, and binary manipulators. In recent years, he has expanded the scope of his research to include applications of group theory in a variety of engineering disciplines and the mechanics of biological macromolecules.

Dr. Chirikjian is a 1993 NSF Young investigator, a 1994 Presidential Faculty Fellow, and a 1996 recipient of the ASME Pi Tau Sigma Gold Medal.